Vol. 08, No. 1 (2026) 457-468, doi: 10.24874/PES08.01B.004

Proceedings on Engineering Sciences

www.pesjournal.net

INFLUENCE OF FRACTURING ON SLOPE STABILITY

Ahmed Hemed[1]

Received 07.05.2025.
Revised 23.07.2025.
Accepted 07.08.2025.

Keywords:

M'HAOUDATT, Slope stability, Open pit, BIF, Planar failure, Wedge failure

A B S T R A C T

Geological investigations indicate that the studied deposit is affected by intense natural fracturing. The stratified rock mass is intersected by several families of diaclases with variable orientations and rough discontinuity surfaces. The orientation of these fractures relative to bench faces significantly influences slope stability by modifying the effective dip in relation to the mining direction. Located in a highly fragmented rock mass, the M'HAOUDATT open pit experiences stability problems that directly affect the strip ratio and the overall production chain. Structural assessment of the pit was conducted using field observations and mine design parameters defined by mining engineers. A kinematic stability analysis was performed to identify potential failure mechanisms based on discontinuity data collected during site investigations. Failure to properly identify structural features such as diaclases, faults, stratification planes, and schistosity can lead to instability issues. In this context, seismic geophysical methods are evaluated as effective tools for slope stability analysis, as they provide mechanical parameters essential for stability calculations. This study aims to determine fracture orientations in different pit sectors to assess their impact on stability and propose measures to restore an optimized strip ratio.

1. INTRODUCTION

Fractures resulting from fracturing always cause significant stability problems. This justifies the importance of the distinction between fracturing induced by mining operations and natural fracturing (Asry et al., 2012). The phenomena of instabilities affect the strip ratio of the mine by the addition of extra tonnage, which is considered a loss of production, especially in the deposit of poor ground holding (Naithani et al., 2017; Reynolds, 1997). Many problems of slope stability require for their resolution, a good knowledge of the state of fracturing to which the rock mass is subjected (Zhang & Li, 2017). The slopes of the M'HAOUDATT pit are unstable due to the non-control of natural fracturing and the absence of underground observations. To develop a geotechnical structural design for the open pit slope (Deng et al., 2020), a geotechnical structural design was developed by evaluating face mapping and data logging together with visual information collected on site. The evaluation of rock slope stability involves many types of uncertainties, such as input parameter uncertainty, calculation uncertainty, and procedure uncertainty. Slope stability analysis can be classified as deterministic or probabilistic analysis depending on how uncertainty is incorporated and evaluated. During the data evaluation, the discontinuity

[1] Corresponding author: Ahmed Hemed
Email: ouldhemed@gmail.com

orientation of the walls and exposed faces is assessed. The kinematic evaluation of slope failure mechanisms expected is based on visual observations on the exposed faces of the pit and the structural data collected during the face mapping exercise (Ahmed & Ouadif, 2023; Cai et al., 2022). The slope stability evaluation was also aided by the use of geo-mechanic parameters. The influence of the soil parameters of the M'HAOUDATT pit plays a primordial role in its state of instability, the presence of water and the cohabitation with air in the pores of the pit takes various forms of penetration in the multiple fractures present in the pit's walls. Validating and interpreting data using bibliographic analysis and fieldwork, which includes structural observations and in-situ measurements (Zhou et al., 2019).

The geophysical methods described are readily available and can help geologists and geotechnical engineers obtain the material properties and boundaries of sub-surface materials.

2. CASE STUDY: DEPOSIT OF M'HAOUDATT

The M'HAOUDATT deposit is located 60 km northeast of Zouerate city (see Figure1). It forms part of a chain 18 km long and 1 km wide, oriented NNW. Almost all of the chain is composed of BIF, with a few units of quartzite. The regional magnetic data shows that the BIF units extend for another 15 km to the SSE (Hemed et al., 2023).

After excavation, instabilities began to appear on the walls of the M'HAOUDATT pit, following the extent of the joints, which caused planar slides on the walls of the pit. This slide is due to poor excavation practices. Above the mining activity, the pit wall has experienced a slide. This instability led to the destruction of the main pit haul road, necessitating the construction of a new road outside the pit, which resulted in a critical increase in the strip ratio, as shown in Figure 1.

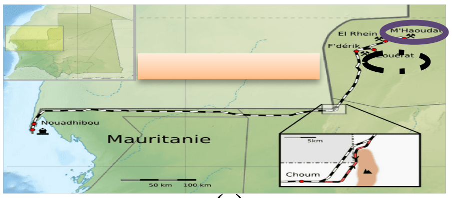

(a)

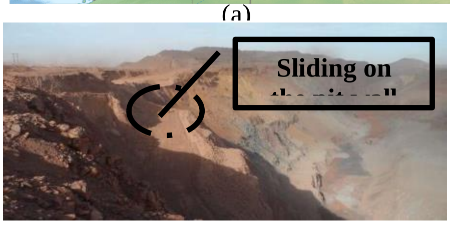

(b)

Figure 1. (a) Geographical location of M'HAOUDATT; (b) view of the M'HAOUDATT pit showing the sliding on the pit wall

The fronts of M'HAOUDATT pit are naturally fractured (presence of discontinuities in the massif: families of diaclases, faults, schistosity, sedimentary joints, etc....) and artificially cracked (effects of shock waves resulting from the volume blasting).

3. STRUCTURAL EVALUATION

The structural evaluation of the proposed pit was based on the data collected during the cells survey, the data from these surveys are integrated to establish a global investigation of the M'HAOUDATT pit.

The cells are presented in Figure 2, with respect to the ultimate pit. Measurements were taken of the orientation and dip of each structural type, as well as the maximum lengths and the number of joints in each joint set, along with the locations of face mapping.

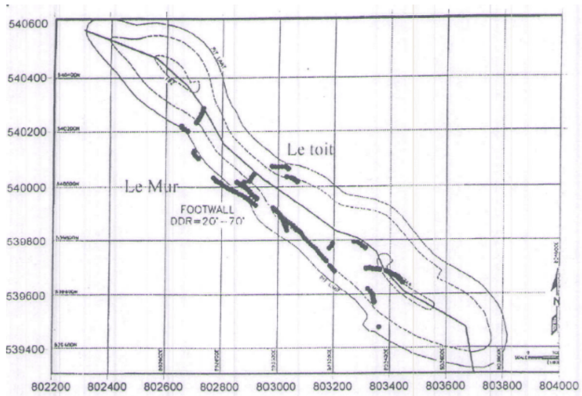

(a)

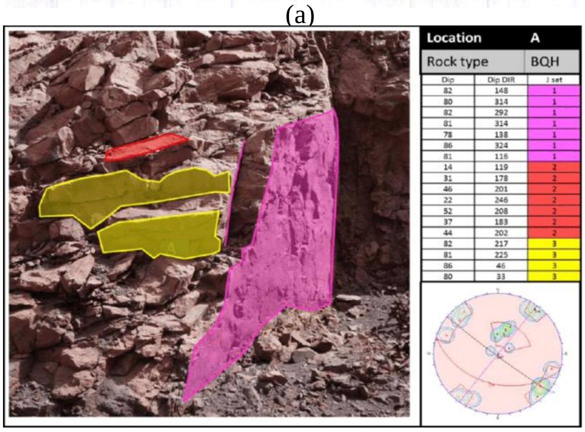

(b)

Figure 2. (a) Location of the cells in the M'HAOUDATT pit; (b) face mapping of the pit wall

The failure mechanisms are defined by a kinematic stability analysis presented below.

4. SEISMIC REFRACTION SURVEY

Geophysical methods can be used to determine the internal structure of soil or rock mass. Various geophysical methods and their advantages for slope stability analysis are discussed. Seismic methods are frequently the most suitable because they rely on the mechanical properties that are also crucial in the mechanical calculation of slope stability analyses. Other geophysical methods, such as electromagnetic, electric resistivity, self-potential, and gravity methods, may be useful to determine the internal structure, but require a correlation of found boundaries with mechanical properties (Liebhardt & Sandmeier, 1996).

Seismic methods are based on measuring an elastic wave (also known as a seismic wave, shock wave, or acoustic wave) traveling through the subsurface. The boundaries where the wave is reflected or refracted are characterized by different densities and/or deformation properties. Seismic methods can almost always be used to determine the internal structure of materials in a slope (Kearey & Hill, 2002).

4.1. Type of waves

Seismic waves may be compression (P-waves), shear (S-waves), or surface waves, such as Raleigh and ground waves. Different properties of the soil or rock mass material have different.

Influences on the behavior of the wave depend on the type of wave. Traditionally, compression (P-) waves were used as they are easy to generate. Compression waves are most sensitive to changes in the normal (compression) stiffness of the materials while shear and surface waves are more influenced by the shear stiffness of the materials through which the wave passes. Shear stiffness is, however, often of greater interest than normal stiffness because it can often be related to the shear strength of sub-surface materials (Liu & Stock, 1993).

Shear wave sources have been inconvenient, but new devices have been created recently (Van Kempen et al., 1998).

4.2. Seismic refraction

Seismic refraction is based on the first arrival of a signal that travels through a layer with a higher velocity. Table.1 gives some characteristic seismic P-wave velocities for sub-surface materials. The method has been standard used for years (Takahashi et al., 2018). Figure 3 shows a simple situation of a more-or-less regular topsoil layer on top of a slightly weathered rock mass on a slope. The first arriving signal at the geo-phones is for the first two geo-phones the direct signal traveling through the topsoil layer and for geo-phones 3 to 12 the refracted wave traveling through the slightly weathered rock mass. For the refracted waves the angle of incidence and angle of refraction equal θ. The topsoil has velocity V1 and the slightly weathered rock mass velocity V2. The angle θ is given by the equation 1:

$$\sin\theta = \frac{V_1}{V_2} \quad (1)$$

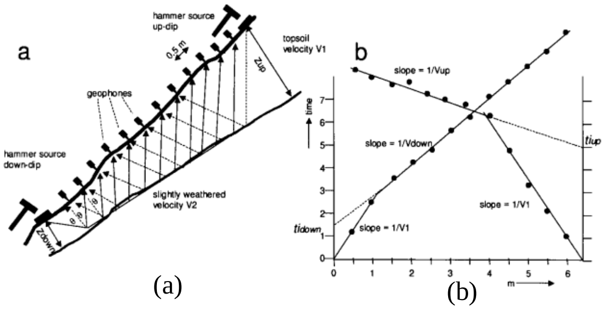

Figure 3. Seismic refraction survey for a boundary parallel to surface. (a) Ray paths, (b) travel time

The thickness of the residual soil layer is determined from Figure 3 in conjunction with equation 2.

$$\text{depth} = \frac{1}{2}\frac{V_1 * t_i}{\cos\left(\text{Arcsin}\left(\frac{V_1}{V_2}\right)\right)} \quad (2)$$

where t_i is the intercept time (Figure 4b).

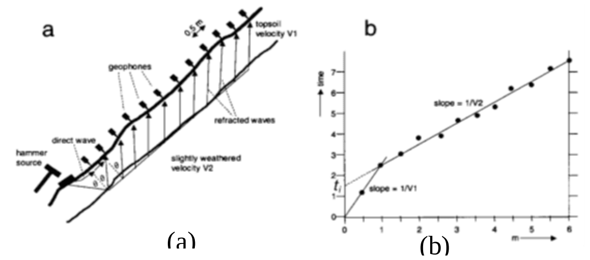

Figure 4. Seismic refraction survey for interface inclined to surface. (a) Ray paths, (b) travel time

For an inclined plane boundary, the survey should be repeated with the source positioned at the opposite end of the geophone spread, as shown in Figure 4. If the inclination between boundary and surface is relatively small, the velocities and depth become (Table 1).

Table 1. Characteristic P-wave velocities ranges

	P-wave velocity (m/s)	Depth (m)
Footwall rock	400–1000	189
Highwall rock	450–3700	175

Seismic reflection

Reflection seismic has a similar set up of source and geo-phones as for refraction seismic surveys, however, not only the first-arrivals are considered, but the complete received signals are incorporated into the interpretation.

Reflection occurs on an interface where the deformation characteristics of soil or rock mass are different on both sides of the interface. This is governed by the so-called 'acoustic impedance' (Z), which equals the product of density and seismic velocity. The 'impedance contrast' in equation 3 is the ratio of the acoustic impedances on both sides of the interface:

$$\delta = \frac{Z_1}{Z_2} \quad \frac{density_1 * velocity_1}{density_2 * velocity_2} \qquad (3)$$

The acoustic impedance and the angle of incidence of the incidence seismic wave govern the energy in the transmitted and reflected waves. The relations between reflected and transmitted energy contents are complicated, but the reflection coefficient in equation 4, is simple for normal incidence (90) of the incident seismic wave (Table 2).

$$\text{Reflection coefficient} = R = \left(\frac{\delta - 1}{\delta + 1}\right)^2 \qquad (4)$$

Table 2. Characteristic P-wave velocities, densities, acoustic contrasts, and reflection

	P-wave velocity (m/s)	Acoustic contrast	Reflection coefficient
Footwall rock	400–1000	1.50	0.040
Highwall rock	450–3700	0.38	0.20

4.3. Measurement of soil and rock properties

Measurement of mechanical properties of soil and rock masses is to a certain extent possible with seismic methods. If P and S waves are measured, a so-called 'seismic E modulus' and 'seismic Poisson's ratio' can be determined:

$$\text{P-wave velocity} = V_p = \sqrt{\frac{\lambda + 2\mu}{\rho}} \qquad (5)$$

$$\text{S-wave velocity} = V_s = \sqrt{\frac{\mu}{\rho}} \qquad (6)$$

$$\text{Seismic Young's modulus} = E = \frac{\mu(3\lambda + 2\mu)}{\lambda + \mu} \qquad (7)$$

$$\text{Seismic Poisson's ratio} = \sigma = \frac{\lambda}{2(\lambda + \mu)} \qquad (8)$$

where λ, μ are Lamé's constants, the density of material.

It is important to understand that these characteristics differ from the Young's modulus and Poisson's ratio that are determined by static or dynamic laboratory or field measurements.

This is because most soil and rock masses exhibit non-linear deformation behavior that varies with frequency. Seismic waves often have different frequencies than dynamic testing, and more significantly, the stress and strain in seismic waves are far lower than those in laboratory or field tests.

The relation between the frequency and the wavelength is:

$$V = f * \lambda \qquad (9)$$

where V, f and λ is the velocity of seismic wave, the frequency and the wavelength.

Inhomogeneities in a soil or rock mass, such as boulders in a soil, joints in a rock mass, will not individually be detected if the wavelength of a seismic wave is low compared to the dimensions of the inhomogeneities. A rule-of-thumb is: if the dimension of the object is more than half the wavelength, it can be recognized as an individual object (whereas the object will not be determined individually if the dimension is less than half the wavelength).

The influence of discontinuities on seismic P-wave velocity has been established empirically by many authors. The relation by Deere et al. relates Rock Quality Designation to seismic velocities measured in the field and in the laboratory (Wang et al., 2020):

$$\left(\frac{V_{field}}{V_{laboratory}}\right)^2 \text{X } 100\% = RQD \qquad (10)$$

V_{field} = seismic velocity measured in the field
$V_{laboratory}$ = seismic velocity measured in the laboratory;
where RQD is the Rock Quality Designation.

The seismic velocity on intact rock is measured in the lab. A signal traveling through unbroken rock as well as through or around discontinuities will have a lower velocity than the velocity measured in the field. It is believed that features like discontinuities have a significant impact on the amplitude of the seismic signal of specific frequencies, even though relatively little research has been done in slope stability studies linking material attributes to attenuation of seismic signals. Although they have not yet been developed, directly applicable techniques should be available soon.

5. KINEMATIC STABILITY ANALYSIS

The collected structural information was compiled and spatially plotted on stereo nets to evaluate the orientation groups.

M'HAOUDATT units are close to the north-west by zones of weakness with exposed joints of the pit wall surrounded by faults and diaclase families.

Shear zones are present within the units, with kinematic indicators along the pit end wall showing a sinistral direction of movement, as illustrated in Figure 5.

Through appropriate software, we have defined four prominent discontinuity sets (Table 3).

Table 3. Summary of major discontinuities identified from the surveys

	Dip	Dip Direction
Foot-wall	65	045
High-wall	72	220
End-wall (North)	67	180
End-wall (South)	82	304

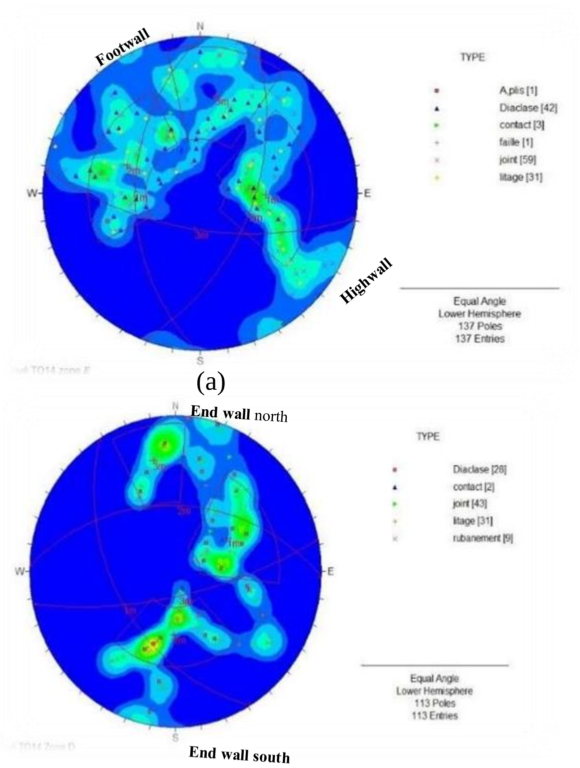

(a)

(b)

Figure 5. (a) STERIONET of major discontinuity sets identified on the walls; (b) STERIONET of major discontinuity sets identified on the End walls

The relevant program to verify each zone's mode of failure mechanism examines the sets in Table 3.

Planar and wedge failure mechanisms were identified as likely to occur along the slope sectors established for the preliminary slope sectors after the primary study of various failure mechanisms.

A preliminary pit design served as the basis for defining the slope sectors in Figure 6. The preliminary sectors and discontinuities data gathered during the pit visit served as the basis for this research.

Due to the variation in face orientation, these studies were developed independently on the pit's sectors (Wang et al., 2022).

Planar failure is the most likely to occur along the pit wall, according to the structural parameters that were assessed for the several failure mechanisms seen on the walls of the M'HAOUDAT pit.

Only plane and wedge failure mechanisms are identified as probable to occur along the slope sectors indicated by the M'HAOUDATT pit as a result of the primary sets, which are outlined in Table 4.

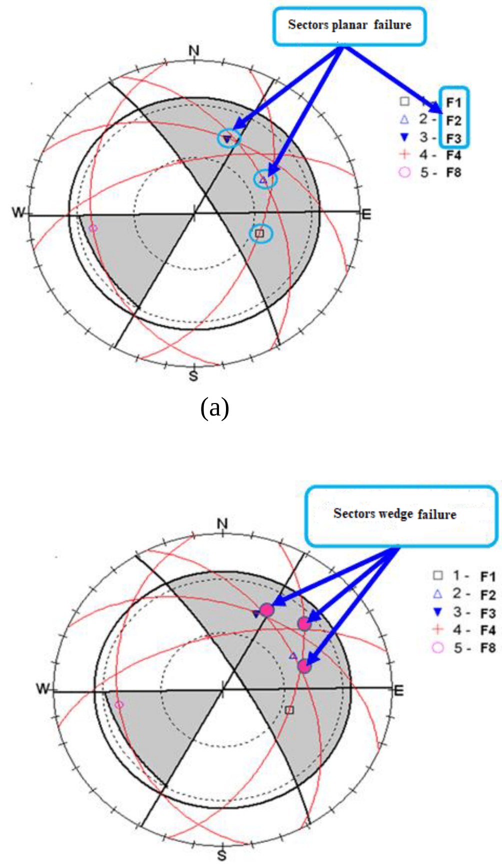

(a)

(b)

Figure 6. (a) Combinations of discontinuities of planar failure; (b) combinations of discontinuities of wedge failure

Table 4. Summary of slope failure risk as per kinematic evaluation

Sector	% Likelihood Of Failure	
	Planar Sliding	Wedge Failure
Foot-wall	19	0
High-wall	3	12
End-wall (North)	8	1
End-wall (South)	2	9

5.1. Interpretation of fracturing analysis

The footwall of the M'HAOUDATT pit exhibits several intersections of discontinuity planes that run parallel to the pit slope, as shown in Figure 7(a). Based on the projection of the discontinuity structures in the analysis of the pit high wall, it is possible that faces where the intersections of these discontinuity planes daylight in the direction of the pit slope may be unstable, as illustrated in Figure 7(b).

(a)

(b)

Figure 7. Examples of planar and wedge failures in M'HAOUDATT pit: (a) Planar failure on the M'HAOUDATT pit footwall; (b) Wedge

5.2. Slope stability evaluation

In all sectors, the M'HAOUDATT pit is operated with a bench face angle not exceeding 70°, as shown in Figure 8(b). This design was developed based on incomplete geotechnical data, including the geo-mechanical parameters of the pit material and the structural model (Chimmani & Lokhande, 2021).

As part of the stability assessment, a pit topographic survey was conducted at the end of March. To evaluate the factor of safety using the limit equilibrium method, the current pit slopes were reconstructed, as illustrated in Figure 8(c).

The pit is utilized at a bench face angle about 81°, which is more than the dip of the pit's discontinuity family, as demonstrated by the cross-section 1 (Table 4).

To measure the FOS of the existing pit, this bench face angle is subject to a limit equilibrium analysis.

As a result, we make our mining operations unsafe by ignoring the safety screen created by families of discontinuities in a rock mass (Table 5).

Table 5. Pit FOS

	FOS
Pit Sectors	0.898

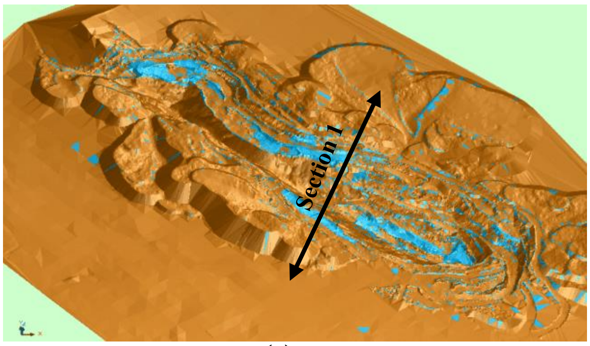

(a)

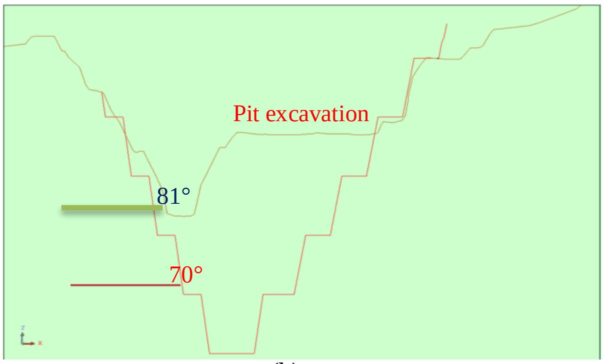

(b)

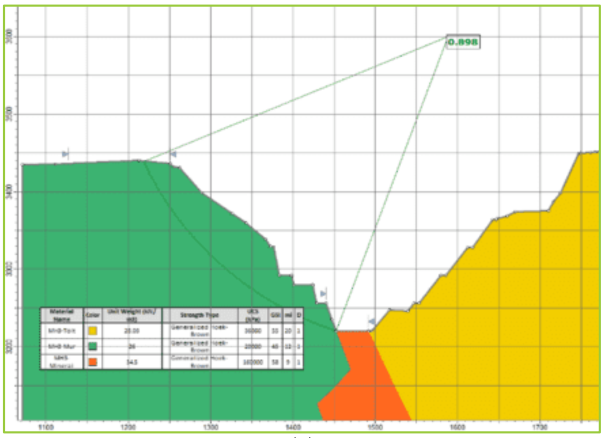

(c)

Figure 8. (a) M'HAUDATT pit state at March 2021; (b) Cross section 1; (c) Simulation result using the limit equilibrium method (cross-section 1)

5.3. Impact of slope failure

A number of fractures that are conducive to various kinds of instability, as the site observation verified impacts the M'HAOUDATT pit.

Joint spacing, filling, and the presence of water between faults are the primary effects of fracturing on the mechanical behavior of the M'HAOUDATT pit massif (Yin et al., 2019).

During the exploitation phase of the M'HAOUDATT pit, non-compliance with the designed bench face angles was observed. As a result, the slopes are more susceptible to sliding, as the pit slope angle exceeds the dip of the discontinuity sets, as shown in Figure 9.


(a)


(b)

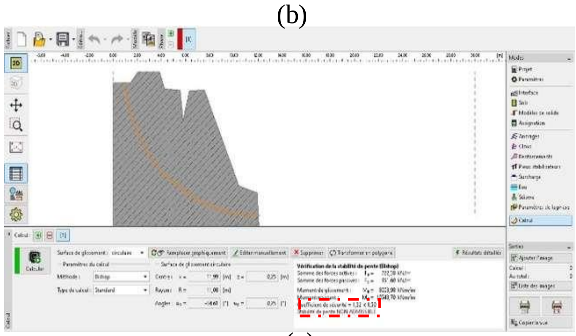
(c)

Figure 9. Examples of instabilities on the pit slopes: (a) appearance of the fracture on the pit walls (after 5 day); (b) appearance of the fracture on the pit walls (after 1 month); (c) simulation of foot-wall with fracture;

A few weeks after the excavation of the pit benches involving a substantial tonnage, signs of instability became apparent, as shown in Figure 10.

The blast's vibrations on the pit wall would have caused it to expand (Morgan & Henrion, 1990).

Following this instability observation, the M'HAOUDATT pit announces that it requires prompt treatment to restore the slopes and reduce the strip ratio of its exploitation (Taylor, 1990).


(a)


(b)

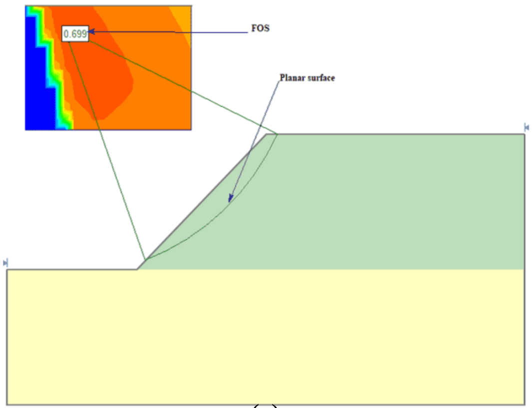

(c)

Figure 10. Examples of instabilities on the pit slopes: (a) destruction of the pit access; (b) Removal of rock blocks; (c) simulation of high-wall

6. PIT SLOPE TREATMENT

To stabilize the slope and increase the factor of safety (FOS), a remediation program was implemented over an eight-month period, involving the removal of approximately 700 KT of material over a depth of 36 m and a width of 50 m, as shown in Figure 11.

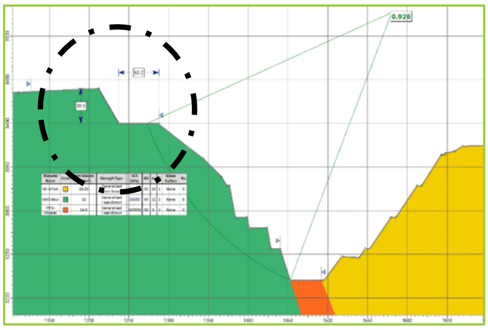

(a)

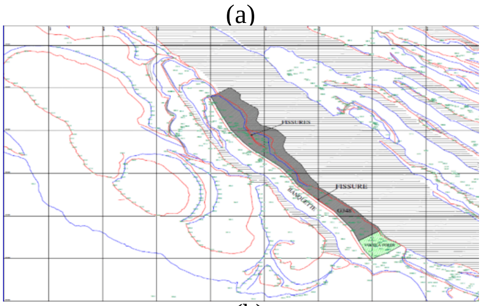

(b)

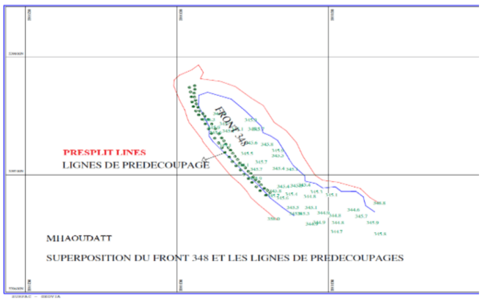

(c)

Figure 11. Unstable slope treatment plan: (a) Simulation of treated slopes using the limit equilibrium method; (b) first cut-polygon; (c) protection presplit line;

6.1. Treatment result discussion

This treatment consists in stripping the detached terrain of the pit deposit, in order to find a stable base to re-exploit the benches considering the dip of structural families, as shown in Figure 12.

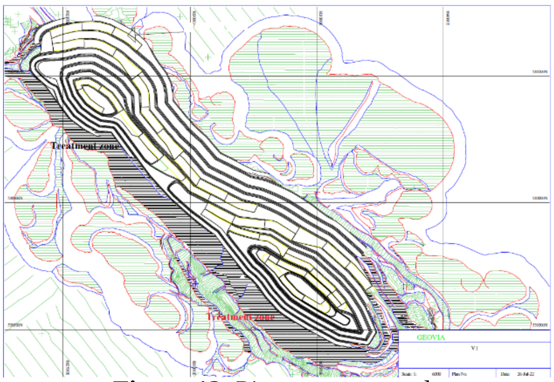

Figure 12. Pit treatment results

The FOS approaches unity at the end of this treatment (Table 6).

Table 6. Pit treatment FOS

FOS before	FOS after
0.8	0.9

After taking a structural reading of the exposed faces, the slopes in the M'HAOUDATT pit require to be resized. To preserve the stability of the pit slope, a kinematic study will be conducted further.

7. PIT RESIZING

The M'HAOUDATT pit's resizing will depend on the pit faces' updated fracture condition. To regulate this phase, we will partition the pit based on the interpretation of the failure mechanisms of the earlier simulation results (Wang et al., 2015). Figure 13 illustrates the high wall and southern end wall in the western section, as well as the footwall and northern end wall in the eastern section.

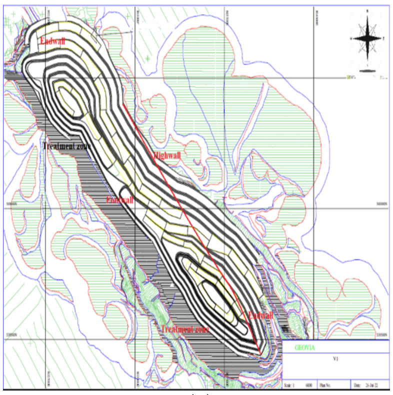

(a)

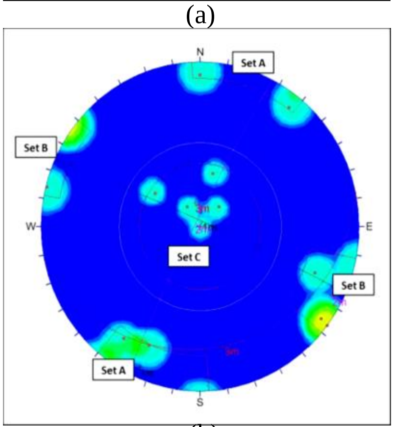

(b)

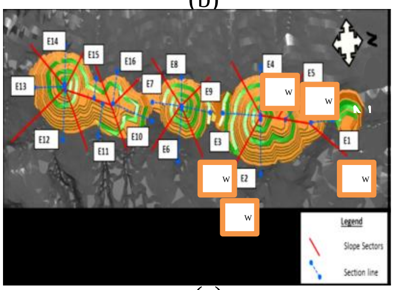

(c)

Figure 13. Structural division of the pit: (a) Pit sectors; (b) Stereo net of identified Major Discontinuity Sets; (c) Slope design areas defined for the pit

We have not recorded any serious changes to the main sets defined in Figure 13, resulting only in planar and wedge failure mechanisms being defined as likely to occur along the pit slope.

A deterministic slope stability evaluation was conducted for the western and eastern sectors, respectively, as presented in Table 7.

Table 7. Results of the kinematic slope failure of the eastern part

	Dip	DDR	PEP	WEP	TFP
W1	62	220	Yes	No	No
W2	58	210	Yes	No	no
W3	62	65	No	No	Yes
W4	62	285	Yes	No	No
W5	72	243	Yes	No	No
E6	58	261	Yes	No	No
E7	62	245	Yes	No	No
E8	72	213	Yes	No	No
E9	58	258	No	Yes	No
E10	72	145	Yes	No	No
E11	72	263	Yes	No	No
E12	58	278	No	Yes	No
E13	62	269	No	No	Yes
E14	58	247	Yes	No	No
E15	62	264	Yes	Yes	No
E16	62	231	Yes	No	Yes

7.1. Pit Resizing results discussion

Due to the weaker schist that is anticipated in this area, the West Pit sector has been divided into two sections. The geological model created for the two deposits was solely focused on mineralogy rather than lithology (Gangi, 1978; Griffith & Taylor, 1921).

Observations in the current M'HAOUDATT pit are consistent with the assessment of possible slope collapse processes. Planar failure along steeply dipping discontinuities (sets A and B) is observed in this area, with the western portion exhibiting potential wedge failure zones, while the eastern portion shows discontinuities parallel to the excavation, as illustrated in Figure 13.

Therefore, the slope stability of both parts will be primarily influenced by the relative orientation of pit slopes at primary discontinuities and laminations. Where possible, the pit slope walls should be parallel to the two main high slope discontinuities (sets A and B).

Based on the new fracture condition according to the results of the previous analysis of the pit, the new pit dimension is summarized in Table 7.

7.2. Slope stability evaluation

The new west pit bench face angle has been evaluated by the limit equilibrium method, as shown in Figure 14.

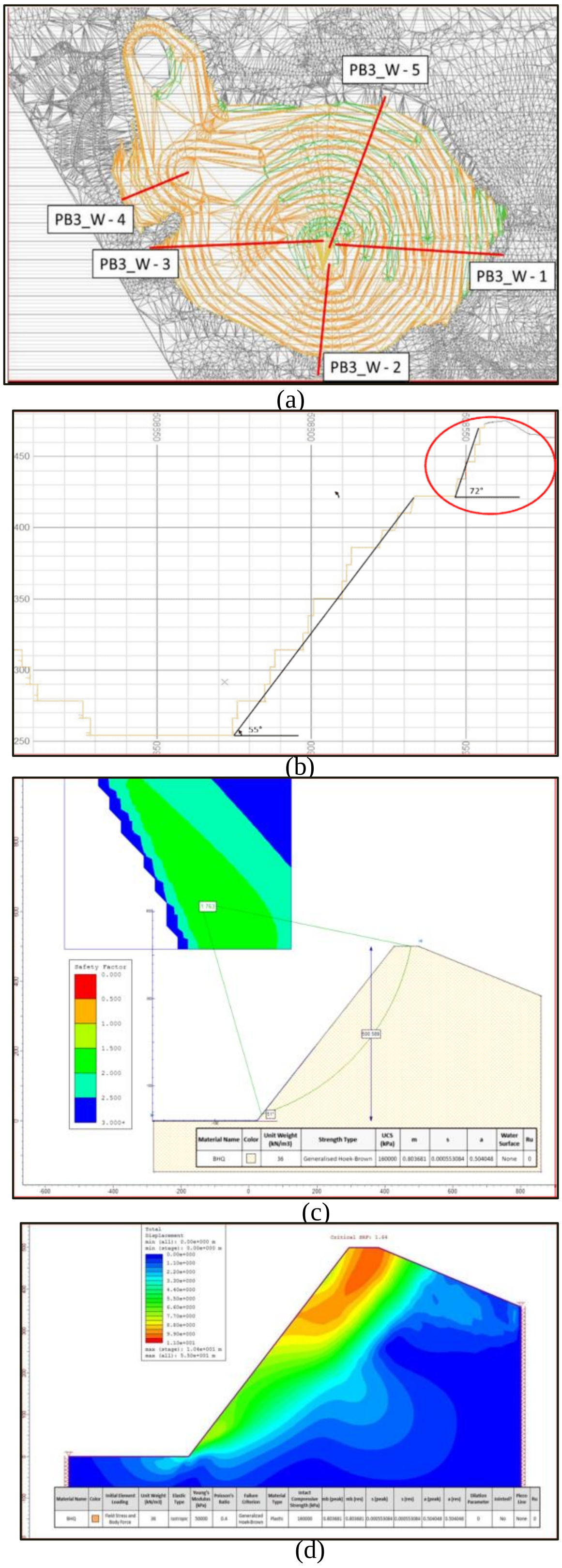

Figure 14. West pit sector benches' evaluation: (a) West pit sector evaluation sections; (b) West pit bench cross section (PB3_W1_W3); (c) Results of Limit Equilibrium Analysis cross section (PB3_W5); (d) Results of Limit Equilibrium Analysis cross section (PB3_W1)

The east pit sector face angle has been evaluated by the limit equilibrium method, as shown in Figure 15.

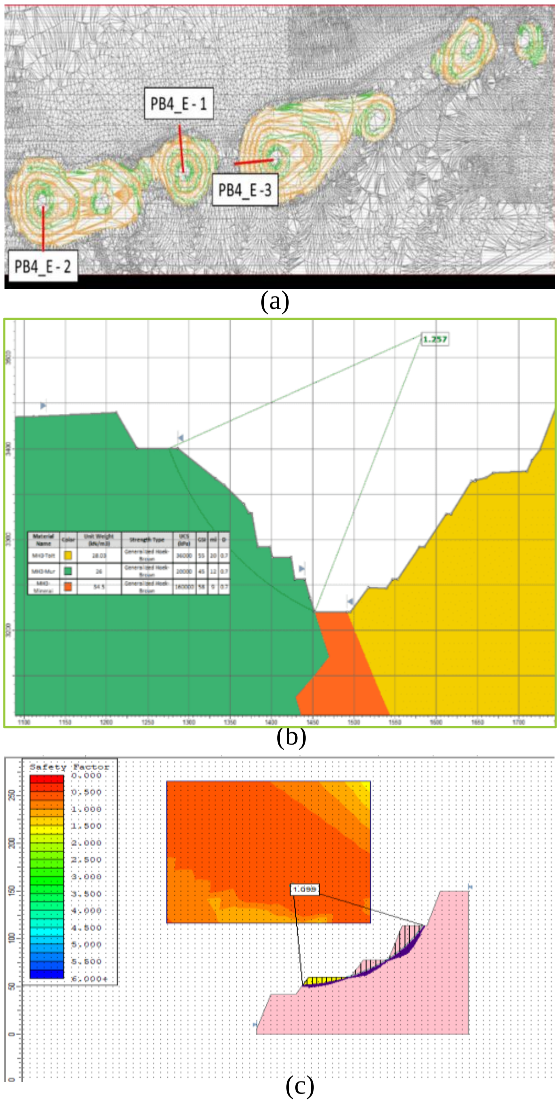

Figure 15. East pit sector face evaluation: (a) East pit evaluation sections; (b) Results of Limit Equilibrium Analysis cross section (PB4_E-1_E-3); (c) Results of Limit Equilibrium Analysis cross section (PB4_E-2)

The factor of safety calculated using the limit equilibrium method at the end of this design is considered acceptable, provided that the mining operation complies with the pit bench face angles specified in Table 8.

Table 8. Pit result FOS

Pit sectors	FOS	Bench face angle
Foot-wall	1.257	62
High-wall	1.763	72
End-wall (north)	1.099	62
End-wall (south)	1.64	72

8. RESULTS AND DISCUSSION

The schistosity of the pit wall requires careful handling when excavating the fronts, although this is not the case when the M'HAOUDATT pit is exploited due to the crucial bench height and lack of safety berms.

In order to capture the feet of the families of discontinuities, it is advised that the bench slope doesn't exceed 62° with a large breadth. The pit foot-wall only has planar failure, according to the diagram projections.

The high wall of the pit has a 72° dip of discontinuities. The main structures on the high wall are represented by three families of diaclases. The stability is primarily controlled by the orientation of the structures and their intersections with each other concerning the direction of the front. The types of fractures that are always associated with the high wall of the M'HAOUDATT pit are wedge failure and toppling fractures.

As the pit is deepened, the main joints at the bottom of the pit are causing significant stability problems. It should always be noted that it is strictly non-recommended for the bench slopes to exceed the dip of the safety screen formed by the natural fracturing.

Thus, it is evident that fracturing causes damage to the fractured massif and enhances detonation in the massif, as evidenced by instability phenomena that start to show up on the pit walls (such as haul road destruction and fractures appearing in very big apertures, etc.). We found that this damage is located in the area where the natural fracturing depression was overlooked.
To regulate the structural direction, the M'HAOUDATT pit is examined as two separate pits. No zones where possible slope stability issues could arise have been discovered, and the plan adheres to the slope angles advised by the families of discontinuities that primarily occur on the pit benches.

Following treatment to address the pit's structural condition, we observed a notable improvement in the FOS of two pits under analysis. The results are acceptable as long as this factor is greater than unity, even though there is less in the eastern region where the damage was notable.

9. CONCLUSION

Due to the absence of a structural model and the complex, variable depth of the pit, understanding the state of natural fracturing in the M'HAOUDATT pit was particularly challenging.

This analytical study aimed to highlight the various fracture orientations encountered, the impact of voids created by mining activities, and the risks associated with neglecting the orientation of discontinuities within the deposit. A rigorous structural investigation combined with pit deepening would have made it possible to identify potential slope instability issues at an earlier stage.

It is therefore strongly recommended to pay close attention to minor instabilities and to continue monitoring ground fracturing conditions in order to identify potential sources of slope instability and prevent larger-scale movements.

References:

Ahmed, H., & Ouadif, L. (2023). Pre-split performance evaluation. *JP Journal of Heat and Mass Transfer, 31*, 19–31. http://dx.doi.org/10.17654/0973576323002

Asry, Z., Samsudin, A. R., Yaacob, W. Z., & Yaakub, J. (2012). Geoelectrical resistivity imaging and refraction seismic investigations at Sg. Udang, Melaka. *American Journal of Engineering and Applied Sciences, 5*(1), 93–97. https://doi.org/10.3844/ajeassp.2012.93.97

Cai, C., Li, B. R., Zhang, Y. Y., He, W., Yang, Y. X., Kang, Y., & Wu, J. W. (2022). Fracture propagation and induced strain response during supercritical CO2 jet fracturing. *Petroleum Science, 19*(4), 1682–1699. https://doi.org/10.1016/j.petsci.2022.03.019

Chimmani, K. V., & Lokhande, R. D. (2021). Study the behaviour of underground oil cavern under static loading condition. Geotechnical and Geological Engineering. https://doi.org/10.1007/s10706-021-01939-0

Deng, X. J., Yuan, Z. X., Lan, L. X., Wit, B. D., & Zhang, J. W. (2020). Roof movement and failure behavior when mining extra-thick coal seams using upward slicing longwall-roadway cemented backfill technology. *Advances in Materials Science and Engineering, 4*, 1–15. https://doi.org/10.1155/2020/5828514

Gangi, A. F. (1978). Variation of whole- and fractured-porous-rock permeability with confining pressure. International *Journal of Rock Mechanics and Mining Sciences & Geomechanics Abstracts, 15*(5), 249–257. https://doi.org/10.1016/0148-9062(78)90957-9

Griffith, A. A., & Taylor, G. I. V. I. (1921). The phenomena of rupture and flow in solids. *Philosophical Transactions of the Royal Society of London Series A, 221*, 163–198. https://doi.org/10.1098/rsta.1921.000

Hemed, A., Ouadif, L., & Baba, K. (2023). Effect of overstress on slope stability in a fractured massif. In K. Baba, L. Ouadif, A. Nounah, & M. Bouassida (Eds.), *Advances in research in geosciences, geotechnical engineering, and environmental science.* GeoME 2023 (Springer Proceedings in Earth and Environmental Sciences). Springer, Cham. https://doi.org/10.1007/978-3-031-49345-4_27

Kearey, P., Brooks, M., & Hill, I. (2002). *An introduction to geophysical exploration* (3rd ed.). Wiley. https://doi.org/10.1002/9781118684980

Liebhardt, G., & Sandmeier, K.-J. (1996). Application of different interpretation methods for seismic refraction data. Proceedings of the 58th EAGE Conference and Exhibition (Paper CP-48-00200). https://doi.org/10.3997/2214-4609.201408789

Liu, C., & Stock, J. M. (1993). Quantitative determination of uncertainties in seismic refraction prospecting. *Geophysics, 58*, 553–563. https://doi.org/10.1190/1.1443438

Morgan, M., & Henrion, M. (1990). The propagation and analysis of uncertainty. In M. Henrion & M. G. Morgan (Eds.), *Uncertainty: A guide to dealing with uncertainty in quantitative risk and policy analysis* (pp. 172–219). Cambridge University Press. https://doi.org/10.1017/CBO9780511840609.009

Naithani, A., Singh, L., & Jain, P. (2017). Rock mass characterization and support design for underground additional surge pool cavern—A case study, India. *Geomaterials, 7*, 64–82. https://doi.org/10.4236/gm.2017.72006

Reynolds, J. M. (1997). *An introduction to applied and environmental geophysics* (1st ed.). Wiley-Blackwell. https://doi.org/10.1002/9780470517910

Takahashi, Y., Sasaoka, T., Sugeng, W., Hamanaka, A., Shimada, H., Saburi, T., & Kubota, S. (2018). Study on prediction of ground vibration in consideration of damping effect by fragment in the rock mass. Journal of Geoscience and Environment Protection, 6, 1–11. https://doi.org/10.4236/gep.2018.66001

Taylor, R. (1990). Interpretation of the correlation coefficient: A basic review. *Journal of Diagnostic Medical Sonography, 6*, 35–39. https://doi.org/10.1177/875647939000600106

Van Kempen, M. H., Drijkoningen, G. G., Nijhof, V., Ter Burg, T., & Roy-Chowdhurry, K. (1998). Comparison of shallow P- and S-wave seismic at the Huesca fluvial fan system in Spain. Proceedings of the 60th EAGE Conference and Exhibition (Paper CP-110-00220). https://doi.org/10.3997/2214-4609.201408319

Wang, C. G., Shi, X. K., Zhang, W., Elsworth, D., Cui, G. L., Liu, S. Q., Wang, H. X., Song, W. Q., Hu, S. T., & Zheng, P. (2022). Dynamic analysis of heat extraction rate by supercritical carbon dioxide in fractured rock mass based on a thermal-hydraulic-mechanics coupled model. *International Journal of Mining Science and Technology, 32*(2), 225–236. https://doi.org/10.1016/j.ijmst.2021.12.004

Wang, H. Z., Li, G. S., Shen, Z. H., Tian, S. C., Sun, B. J., He, Z. G., & Liu, P. Q. (2015). Experiment on rock breaking with supercritical carbon dioxide jet. *Journal of Petroleum Science and Engineering, 127*, 305–310. https://doi.org/10.1016/j.petrol.2015.01.006

Wang, X. F., Wang, X. L., Wang, J. Y., & Tian, Z. X. (2020). Feasibility study and prospects of rock fragmentation using ultrasonic vibration excitation. *Applied Sciences, 10*(17), 5868. https://doi.org/10.3390/app10175868

Yin, D. W., Chen, S. J., Li, B., & Guo, W. J. (2019). Bed separation backfill to reduce surface cracking due to mining under thick and hard conglomerate: A case study. *Royal Society Open Science*, *6*(8), 190880. https://doi.org/10.1098/rsos.190880

Zhang, J. W., & Li, Y. L. (2017). Ultrasonic vibrations and coal permeability: Laboratory experimental investigations and numerical simulations. *International Journal of Mining Science and Technology*, *27*(2), 221–228. https://doi.org/10.1016/j.ijmst.2017.01.001

Zhou, T., Zhu, J. B., Ju, Y., & Xie, H. P. (2019). Volumetric fracturing behavior of 3D printed artificial rocks containing single and double 3D internal flaws under static uniaxial compression. *Engineering Fracture Mechanics*, *205*, 190–204. https://doi.org/10.1016/j.engfracmech.2018.11.030

Ahmed Hemed
3GIE Laboratory, Mohammedia
Engineering School,
Rabat,
Morocco
ouldhemed@gmail.com
ORCID 0000-0002-9398-2618